Bioprintable, stiffness-tunable collagen-alginate microgels for increased throughput 3D cell culture studies.

Carley Ort[1], Yimai Chen[1], Ajinkya Ghagre[3], Allen Ehrlicher[2-6] and Christopher Moraes[1,2,4*]

[1] Department of Chemical Engineering, McGill University, 3610 rue University, Montreal, QC, Canada.
[2] Department of Biomedical Engineering, McGill University, 3775 rue University, Montreal, QC, Canada.
[3] Department of Bioengineering, McGill University, 817 Sherbrooke Street West, Montreal, QC, Canada.
[4] Rosalind and Morris Goodman Cancer Research Center, McGill University, Montreal, QC, Canada.
[5] Department of Anatomy and Cell Biology, McGill University, Montreal H3A 0C7
[6] Department of Mechanical Engineering, McGill University, Montreal H3A 0C3

* corresponding author
E-mail: chris.moraes@mcgill.ca

Keywords: high throughput, biomaterial, stiffness, mechanobiology, cell culture

Abstract:

3D culture platforms with tunable stiffness have the potential to improve many applications such as drug discovery, organoid studies, and stem cell differentiation. Both dimensionality and stiffness regulate crucial and relevant cellular processes. However, 3D culture models are often limited in throughput and difficult to adopt for widespread use. Here, we demonstrate an accessible 3D, stiffness-tunable tissue culture platform, based on an interpenetrating network of collagen-1 and alginate. When blended with polymers that induce phase separation, these networks can be bioprinted at microliter volumes, using standard liquid handling infrastructure. We demonstrate robust reproducibility in printing these microgels, consistent tunability of mechanical properties, and maintained viability of multiple printed cell types. To highlight the utility and importance of this system, we demonstrate distinct morphological changes to cells in culture, use the system to probe the role of matrix mechanics and soluble factors in a collagen contraction assay, and perform a prototype viability screen against a candidate chemotherapeutic, demonstrating stiffness-dependent responses.

Introduction

Three-dimensional biomaterial culture systems have emerged as critically important platforms for in vitro cell-based applications, as dimensionality is an important regular of cell function, influencing morphology, proliferation, and migration, amongst many other cell behaviours.[1] Technological innovations in biomaterial design now afford the ability to tune key microenvironment properties such as binding ligand density and stiffness; variables known to drive cellular function.[2 3 4 5] This is particularly important in models of development, disease, and drug efficacy, as stiffness is now a well-established driver of important cellular processes connected to stem cell differentiation and disease progression.[6 7 8 9] However, conventional culture technologies used in high-throughput applications such as petri dishes, and even spheroid and organoid cultures cannot be easily tuned to manipulate these parameters, as previously reviewed.[10] Hence, the ability to tune stiffness in engineered models may be particularly desirable to advance applications such as drug discovery, personalized medicine, and tissue engineering screening platforms.[11 12 13 14 15 16 10]

Applying these platforms beyond relatively artisanal fundamental studies, and towards industrial-scale screening applications is made difficult by the challenges associated with increased-throughput testing of mechanically-tunable 3D cultures. In general, 3D culture models require large volumes of expensive reagents, high cell quantities, and complex handling procedures; all major drawbacks in fields where cost, speed, and robustness drive culture adoption. Bioprinting is emerging as a useful technique to create simple 3D tissues[17 18 19 20] and we have previously demonstrated the use of aqueous two-phase systems (ATPS) to print microliter volumes of cell-laden collagen hydrogels within a well-plate, using standard liquid handling tools.[21] Printing small volumes is particularly challenging with conventional printing methods, as they are highly sensitive to evaporation, often resulting in low cell viability.[21] This issue is circumvented in the ATPS-collagen system, where gelation of small volumes occurs while submerged, with no gel-to-air interface. Briefly, this is accomplished by inducing phase separation of a collagen pre-polymer during gelation, by incorporating immiscible dextran and polyethylene glycol (PEG) polymers into the two phases. The small-volume gels further allow rapid diffusion and equilibration of large molecules, simplified imaging, reduced reagent consumption, and easy adoption into existing high-throughput workflow infrastructures.

In this work, we build upon our previous studies and demonstrate the ability to precisely control stiffness independently from binding ligand density within this bioprintable collagen system. Interpenetrating networks (IPNs) of alginate with extracellular matrix (ECM) have previously been used to control stiffness of engineered cultures with great success.[2 22 5 23 24 25 26 27] Alginates are biocompatible polysaccharide polymers that can be crosslinked using cell-friendly divalent ions such as calcium, and present no additional binding sites to cells unless specifically modified to do so.[28] Collagen-1 is the most abundant extracellular matrix protein present in tissue[29] and provides biochemical feedback for cellular processes such as survival and proliferation.[30] Blending these two gels into an IPN with the polymers necessary to induce phase separation should hence provide the ability to tune the mechanical properties of ATPS-bioprintable microgels.

To provide a robust system for increased throughput of 3D, mechanically-tunable cultures (Figure 1), we designed and characterize collagen-alginate IPNs as biomaterials for automated ATPS-based “printing” into microlitre droplets. We demonstrate reproducible microdroplet printing with precise control over storage modulus, and distinctive stiffness-driven morphological phenotypes for breast cancer cells and fibroblasts. As a first application for this platform, a chemotherapy screening assay of breast cancer cells demonstrated the role that stiffness plays in drug response and underscores its placement in high-throughput screening. Finally, contraction assays demonstrated the role of stiffness in these remodellable micro-matrices under contractile stimulating or suppressive conditions.

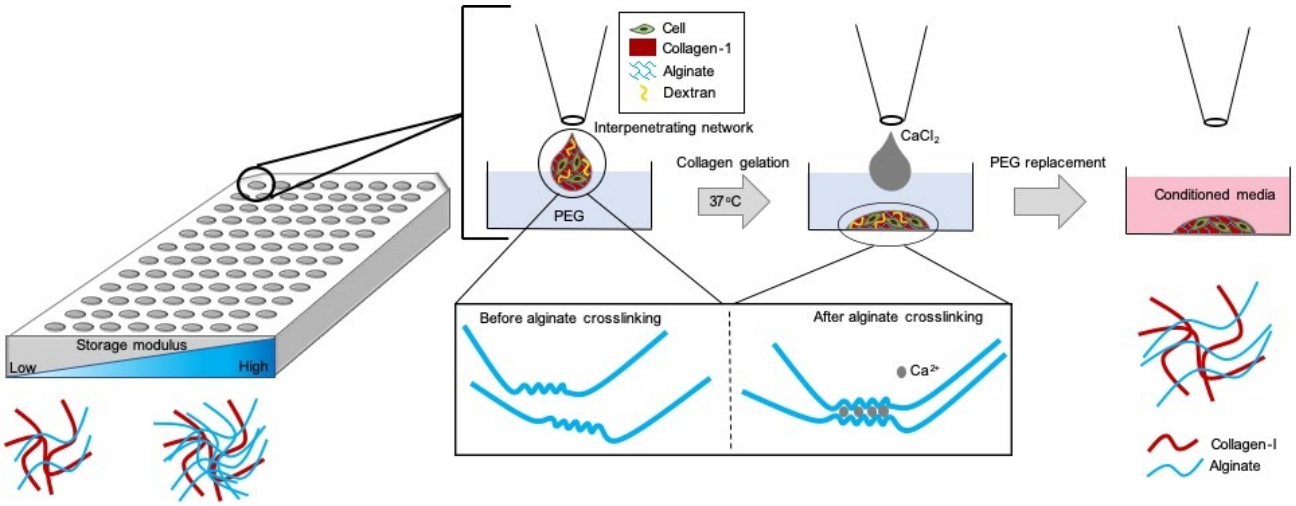

Figure 1. Schematic of the stiffness tunable microgel printing culture platform. Microgel matrices consist of a constant collagen-1 concentration for cell adhesion and increasing alginate concentrations for storage modulus control. Robotic liquid handling pipettes microlitre volumes of the interpenetrating network into PEG and the matrix is thermodynamically gelled. Alginate is ionically crosslinked with calcium ions and PEG is replaced with conditioned media as the final step.

Materials and Methods

Materials

Dulbecco's modified eagle's medium x1, acetic acid, sodium hydroxide, phosphate buffered saline, sodium alginate, poly(ethylene glycol) (PEG) (35K), calcium chloride, dimethyl sulfoxide (DMSO), paclitaxel, pluronic F-108, paraformaldehyde, Triton X-100, Hoechst 33258, phalloidin, ultra-low attachment 96 well flat bottom plates, and goat serum were purchased from Sigma Aldrich (Oakville, ON). Antibiotic antimycotic, type I collagen (5mg/mL), Calcein AM, and ethidium homodimer-1 were purchased from Life Technologies (Carlsbad, CA, USA). HyClone fetal bovine serum, 0.25% trypsin-EDTA, HyClone phosphate buffered saline, cell culture treated 96 well flat bottom plates, and UltraPure distilled water were purchased from Fisher Scientific (Ottawa, ON). Anti-Ki67 antibody and goat anti-rabbit IgG were purchased from Abcam (Cambridge, UK). Dextran (500K) was purchased from Dextran.ca.

Cell Culture

HS5 human fibroblast cell lines and MDA-MB-231 epithelial adenocarcinoms cell lines (ATCC) were cultured in DMEM supplemented with 10% fetal bovine serum (FBS) and 1% antibiotics-antimycotics, and maintained at 37 °C, 5% CO_2. Cells were routinely passaged for seeding experiments or re-plating using 0.25% trypsin-EDTA.

Microgel printing

All handling was carried out under sterile conditions. A dextran-rich gel solution was prepared on ice by adding the following reagents in sequence to a 1.5mL Eppendorf tube: 3mg/mL collagen, diluted down from 5mg/mL in 20mM acetic acid, 1M sodium hydroxide, 10x PBS, 15% dextran dissolved in distilled water, distilled water, alginate of desired concentration, and cell suspension in PBS (see Supplemental Table S1 for volumetric mixing recipes). Cells were added in a PBS suspension to prevent premature calcium addition and alginate gelation. The solution was mixed by pipetting, taking care not to create air

bubbles. A PIPETMAX® (Gilson) automated liquid handling system was loaded with reagents and programmed to dispense the PEG-rich phase and dextran-rich droplets into plasticware. 96-well plates adhesive to adherent cells were used for standard culture experiments, and ultra-low attachment plates were used for collagen contraction experiments. PEG was dispensed into each well of a 96 well plate, followed by a drop of the dextran rich gel solution. Plates were then removed from the PIPETMAX® and gels were incubated at 37 °C for 45 minutes. Calcium chloride was added to all cultures for 5 minutes, at an ~1000x molar excess for alginate crosslinking (0.1 wt%) to saturate crosslinking sites. Calcium was allowed to diffuse for 5 minutes to allow complete alginate crosslinking. Given that maximal diffusion distances are less than 1 mm, small molecules such as calcium, equilibrate near-instantaneously, based on experimental results and computational models previously developed.[21] Samples were either aspirated by hand or serially diluted to replace the PEG media with supplemented media, and cultured at 37 °C, 5% CO_2 during experiments.

Scanning electron microscopy

IPNs were gelled in 250 μLvolumes, rather than using the ATPS method to allow more surface area for handling and imaging. Gels were snap frozen in liquid nitrogen for 1 minute, and lyophilized overnight. Dehydrated ECM was then peeled back with tweezers to uncover more central gel architecture and imaged using a scanning electron microscope (SEM, SU3500, Hitachi Hi Technologies, Tokyo, Japan). Observations were performed under variable-pressure imaging mode (3.0 kV, 30 Pa).

Shear Modulus measurements

150 μL of gel prepolymer was dispensed into 35 mm glass bottom petri dishes containing 1mL of 6 wt % PEG and gelled at 37 °C for 45 minutes. Calcium chloride was then added at a final concentration of 0.1wt% to each dish for 15 minutes to crosslink the alginate. The PEG/calcium chloride suspension was replaced with 1 mL PBS, and left to swell overnight at 4 °C. To mechanically probe the hydrogel at length scales relevant to individual cells, twisting magnetic cytometry was used to measure the micro-scale shear moduli of the gels and this method is discussed elsewhere. [31] Briefly, a ferromagnetic bead 4.5 μm in diameter was depressed into the surface of the gels and subjected to an external magnetic field. This magnetic field caused the beads to oscillate, and the displacement of the beads was used to calculate the shear modulus of the gel.

Cell viability

HS5 viability in 3D gels was examined at day 9 after seeding cells at a density of 250 cells/ μL and MDA-MB-231 viability was examined at day 5 after seeding cells at a density of 200 cells/μL. Viability was visualized by live/dead staining the cells with 2 μM calcein AM and 2 μM ethidium homodimer in supplemented media before image collection.

Cell morphology

To study 2D cell morphology on gel surfaces, 40 μL of cell-free hydrogel IPN solution was added to well in a 96 well plate, gelled at 37 °C, 5% CO_2 for 45 minutes followed by alginate crosslinking with 0.1 wt% Ca Cl2 for 15 minutes. Subcultured HS-5 cells were suspended in supplemented media at low densities of 70 cells/μL, and 50 μL were added to each well. Cells were allowed to attach and spread for 24 hours. Gels were fixed in 4% paraformaldehyde, permeabilized with 0.1% Triton-X and stained with 0.5 μg/mL phalloidin and 1 μg/mL Hoescht to view the F-actin cytoskeleton and nucleus respectively.

HS5 and MDA-MB-231 morphology in 3D gels was analyzed at day 3 after seeding cells at a density of 125 cells/ μL to view single cell morphology before gel contraction. HS5 morphology was also analyzed at day 9 after an initial seeding density of 1000 cells/ μL to view overall tissue architecture following contraction. Gels were fixed in 4% paraformaldehyde, permeabilized with 0.1% Triton-X and stained with 0.5 μg/mL phalloidin and 1 μg/mL Hoescht to view the F-actin cytoskeleton and nucleus respectively.

Microgel contraction analysis

HS-5 cells were printed into 1 μL microgel droplets at a density of 1000 cells/ μL and incubated with either FBS free media, FBS supplemented media, or FBS supplemented media containing 5 ng/mL of TGFβ-1 at 37 °C, 5% CO_2. Microgels were allowed to contract for 6 days and brightfield images of contracting microgels were taken every 24 hours. Media was exchanged every 48 hours.

Drug responsiveness and proliferation analysis

MDA-MB-231 cells were printed into the gels at a density of 200 cells/ μL and incubated with supplemented media at 37 °C, 5% CO_2 for 3 days to allow spreading. For drug responsiveness studies, gels were then treated with 0.1, 1 or 150 μM Paclitaxel in supplemented media. Control gels were given the matched volume of the vehicle (DMSO). After 48 hours cell viability was examined by replacing media with 2 μM calcein AM and 2uM ethidium homodimer in supplemented media. For proliferation studies, gels were fixed on day 3 in 4% paraformaldehyde, permeabilized with 0.5% Triton-X, blocked with 2.5% goat serum, incubated with 1/1000 dilution of Ki67-rabbit antibody, rinsed twice with PBS, blocked again with 2.5% goat serum, incubated with 1/100 dilution of goat-anti rabbit secondary antibody.

Image and Statistical analysis

Fluorescent, brightfield, and phase-contrast images were collected on an Olympus microscope (IX73, using Metamorph software). Percent void space was quantified by applying a consistent threshold value across all images, selected to visually separate the matrix from the background. Area fraction was then measured in ImageJ. All gel areas and cell spread areas were quantified by carefully tracing the outside of the gel or cell using the freehand selection tool in ImageJ software and collecting area from the measurements tab under “Analyze”. Gel circularity was also retrieved in this manner. Cell aspect ratio was collected using the bounding rectangle measurement in ImageJ software. F-actin fluorescent intensity was quantified by sampling the mean gray value of 130μm^2 sections within each microgel using the ImageJ analyze tool, while maintaining consistent staining and imaging parameters. Cell viability and Ki67 staining were both quantified by applying a consistent threshold value across all images, inverting the image, and collecting analyzed particles.

Prism v8.2 (GraphPad Software, San Diego, CA) statistical analysis software was used to calculate one-way ANOVAs between treatment groups, followed by a Tukey post hoc test, carried out at 95% significance. Each well was considered independent for all experiments.

Results

Characterization of printed collagen-alginate IPNs.

Microgel formulations with equivalent collagen content and alginate concentrations ranging from 0 to 1.6 mg/ml were printed at volumes ranging from 0.1 μL to 2 μL (Figure 2A). Volumes larger than 2 μL are also capable of being printed (data not shown). Holding the concentration of collagen constant across the gels controls for binding ligand availability, ensuring that only one variable (storage modulus) is changing at a time. This is important, as it allows the decoupling of stiffness and binding ligand density: two independent drivers of cell behaviour.[32] In using alginate concentration to tune stiffness, alginate crosslinking sites were saturated by exposing microdroplets to excess calcium ions. Due to outside-in alginate crosslinking as calcium ions diffuse, calcium crosslink instability over multiday culture periods,[28] and cell release of calcium into surrounding culture,[33] saturating alginate crosslinks should provide a uniform and stable mechanical profile within the gels. Printed droplets form consistently sized microgels, based on projected area and droplet circularity (Figure 2B,C). Occasional irregularities and gel folding occurs due to media movement during plate handling and can be avoided with careful plate transport before collagen gelation or by gelling on a thermally controlled stage. While the 0.1 μL droplets do demonstrate the low volumes possible with the ATPS technique, some variation was observed at 0.1 μL print volumes, likely because the Pipetmax printing platform is calibrated to reproducibly dispense print volumes greater than 1 μL. Uniformity can hence be improved even at these small volumes by using appropriately rated liquid handling tools. Further, microgels are able to either securely stick to the bottom of the well, or remain free floating in the media depending on the desired application by selecting appropriate plasticware. Bioprinting the microgels into standard plates used for adherent cell culture allows gels to remain adhered on the plastic surface, even after multiple washes in media. In contrast, microgels bioprinted into ultra-low attachment wells results in free floating gels. Plasticware can therefore be selected based on the desired application, allowing further flexibility in using this technique.

As alginate concentration increases within the matrix, pore structure changes, causing total void space to decrease, as evidenced by SEM images of the printed hydrogels (Figure 2D,E). This is expected, as the total polymer concentration increases with increasing alginate content; but it is important to note that cell-adhesive collagen content remains constant across all conditions. We then verified that by changing the concentration of alginate in the IPN, the storage moduli of the microgels could be tuned. Storage moduli of cell-free IPNs ranged from 0.54 ± 0.15 kPa to 2.3± 0.28 kPa between 0 mg/mL and 1.6 mg/mL of alginate (Figure 2F). As storage moduli are subject to change during cell remodelling, only initial mechanical properties are referred to throughout this work. Loss moduli also increased with alginate concentration (Figure S1B), resulting in a consistent elastic to viscous ratio (or phase angle; Figure S1C) between all microgel formulations. Phase angle influences gene expression and inflammatory secretion of mesenchymal stem cells,[34] and was hence controlled for in these experiments. The successful production of microlitre matrix volumes via robotic liquid handling, combined with the flexibility to provide robustly tunable mechanical properties suggests the possibility of a high-throughput 3D, stiffness-tunable culture platform through compatibility with existing high through-put liquid-handling infrastructure.

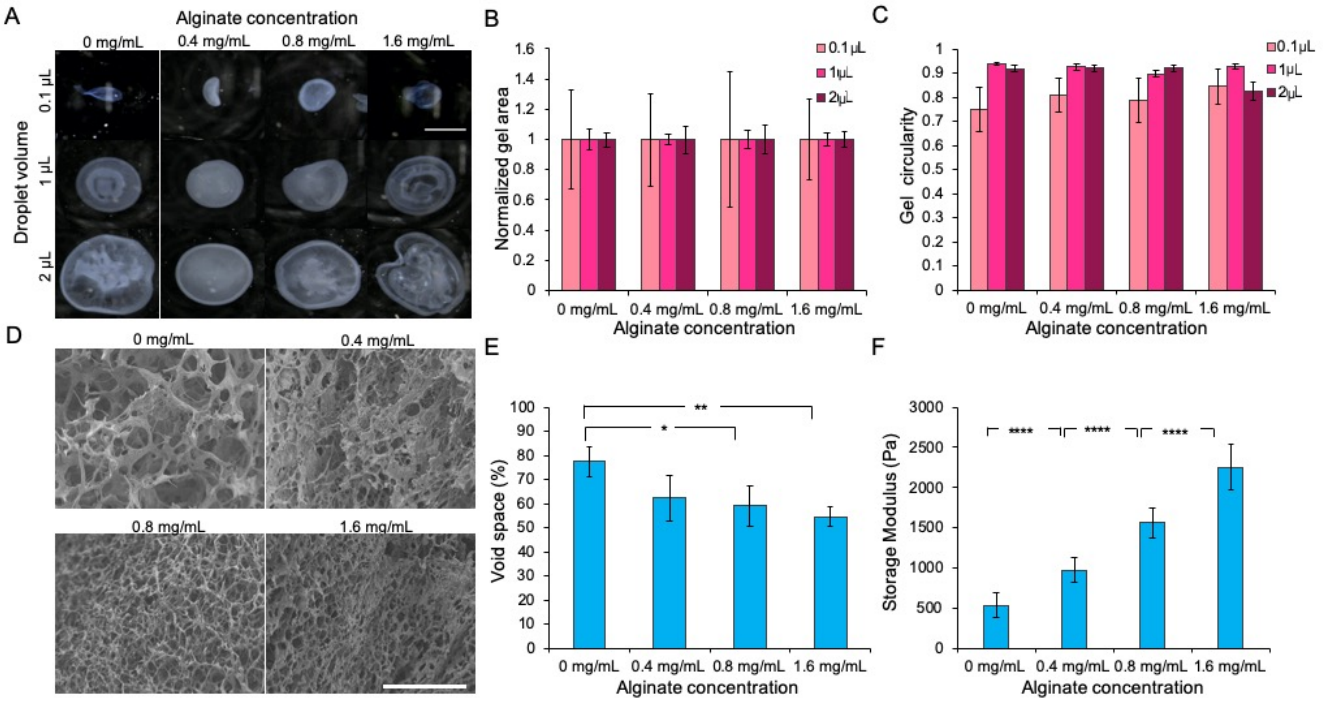

Figure 2. Characterization of printed microgels. (A) Microprinted droplets at different volumes and alginate concentrations. Scale: 1mm. (B) Areas of microprinted droplets at different volumes and alginate concentrations. Areas have been normalized to the average area printed by each corresponding pipette head. (C) Circularity of microprinted droplets at different volumes and alginate concentrations. (D) Scanning electron microscopy images of matrices with increasing concentrations of alginate. Scale: 50 µm. (E) Percent void space of matrices, as a measure of porosity. (F) Storage moduli of matrices, as assessed by optical magnetic twisting cytometry (data presented as mean +/- standard deviation; (E): n = 3; (F): n= 3 gels, minimum of 30 measurements per gel; * $p < 0.05$; ** $p < 0.01$; ****$p<0.0001$, by one-way ANOVA with Tukey post-hoc analysis).

Microgel stiffness influences cell morphology

Cell viability of HS5 fibroblasts immediately following bioprinting was over 95% (Figure S2). Cultured separately, fibroblasts and MDA-MB-231 breast cancer cells displayed high viability for up to nine and five days in culture respectively (Figure 3A,B), at both low (125 cells/ µL) and high cell densities (1000 cells/ µL), demonstrating the platforms utility for longer culture periods and versatile cell densities. The ability to print 3D cultures with as few as 10-100 cells in each sample may have strong potential in personalized medicine applications for which patient cells are both precious and limited.

The morphological behaviours of both HS5 and MDA-MB-231 cell types are well-established, making them ideal candidates to investigate morphology within the microgels. Cell morphology throughout the microgels was readily measured using conventional epifluorescent imaging, as the droplets are sufficiently small to present no challenges in imaging using standard long-working distance objectives. Breast cancer cells displayed two major morphologies (rounded or spindle-shaped) within all four test conditions, giving rise to highly heterogeneous cell aspect ratios (Figure S3). The proportion of spindle-shaped versus rounded breast cancer cells skewed towards rounder cells with increasing initial stiffness (Figure 3C,D). Similarly, high initial microgel stiffness limited spread area of the fibroblast cell line (Figure 3E,F). Although fibroblasts often took on a spindle-shaped morphology (Figure 3E) with similar aspect ratios within the microgels of differing stiffness (Figure S4), the spread area decreased

considerably in all gels stiffened with alginate (Figure 3F). This trend is also noted when fibroblasts are cultured on top of our gels (as in a 2D system), where initially stiffer gels give rise to decreased spread (Figure S5). Morphology also differed between 2D and 3D conditions, where fibroblasts cultured on top of the gels visually displayed higher aspect ratio with lower spread area as compared to 3D culture (Figure S6), further rationalizing the need for 3D culture when conducting morphological analysis.

Increased stiffness also promoted well-defined actin structures in fibroblasts, which were much more diffuse in softer microgels (Figure 3E,G) (Figure S7), consistent with known effects of stiffness on actin fiber formation,[35 36] and suggestive of a more contractile and mechanically-active phenotype within stiffened matrices.

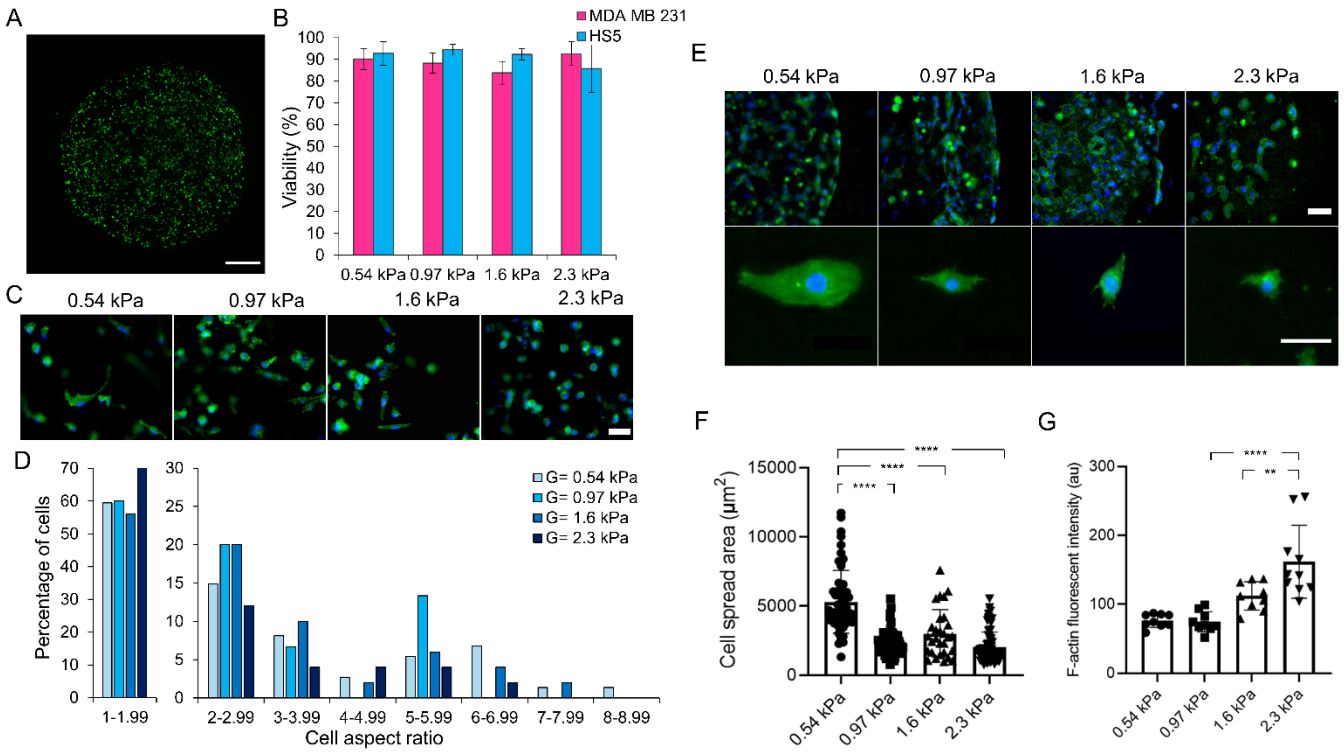

Figure 3. *Morphological characterization of breast cancer cells and fibroblasts in stiffness-tunable microgels. (A) Representative calcein AM (live) and ethidium homodimer (dead) stain of a 0.97 kPa IPN containing HS5 fibroblast cells on day 9 [green: live cell, red: dead cell, Scale: 500 μm]. (B) Quantification of MDA-MB-231 breast cancer cell and HS5 fibroblast viability within the microgels at 5 and 9 days in culture respectively. (C) Morphology of breast cancer cells on day 3 within the microgels of various stiffness and (D) quantitative results of cell aspect ratio. (E) Fibroblast actin architecture, within multicellular tissues at day 9 (top) and single cell fibroblast spread area at day 3 (bottom) of culture within microgels [green: F-actin, blue: nuclei, scale: 50μm]. Quantitative results of (F) single cell spread area and (G) average F-actin fluorescent intensity per 130μm² (data presented as mean +/- standard deviation; (B): n=3 microgels (D): n=3 microgels, 10-30 cells each (F): n=6-12 microgels, 28-84 cells each; (G): n=3 microgels, 3-4 areas each; **p < 0.01; **** p < 0.0001 by one-way ANOVA with Tukey post-hoc analysis).*

Soluble factors can stimulate contractility even in stiffened matrices

Decreases in fibroblast spread area with simultaneous formation of defined architectures suggest opposing effects on contraction of the collagen matrix, a commonly-used assay to assess ECM remodelling.[36] We have previously demonstrated the utility of bioprintable collagen gels as a microscale contraction assay; and noted that small gels allow rapid equilibration of even large-molecular weight soluble factors throughout the gel volume.[21] We hence asked whether tissue contraction was influenced by initial matrix stiffness; and used the small-volume gels to simultaneously understand the effects of soluble cues on this contraction process, using FBS and TGFβ-1 as candidate stimuli, as both are well-established to stimulate collagen contraction in culture.[36] In serum-free media, initially soft microgels contracted faster and to a much higher overall contraction within 6 days than initially stiffened microgels (Figure 4A), demonstrating that alginate stiffens tissues sufficiently to hinder contraction. However, supplementing the media with FBS was sufficient to induce similar degrees of contraction, but at a slower rate (Figure 4B). Further addition of TGFβ-1 prompted no additional contraction, suggesting that factors in serum are sufficient to drive maximal contraction (Figure 4C,D).

This data demonstrates that although the alginate-doped gels are stiffened, they still retain the capacity to be remodelled under appropriate stimulation. It also suggests that contrary to previous suggestions[35] increased tissue stiffness is not sufficient to drive contractile processes in these gels, and that soluble stimuli are still necessary to recreate this phenotype in culture. Additionally, microgel stiffness increases across contraction.[37] As such, microgel stiffness is dynamic and can only be guaranteed immediately following gelation. The change in gel stiffness in real-time, along with how instantaneous stiffness influences cell behaviours such as contraction and proliferation are intriguing questions. More broadly, this experiment demonstrates the utility of the stiffness-tunable bioprintable microgels as a miniaturized collagen contraction assay to simultaneously probe the effects of matrix stiffness and soluble stimuli on this important developmental and disease-related process.

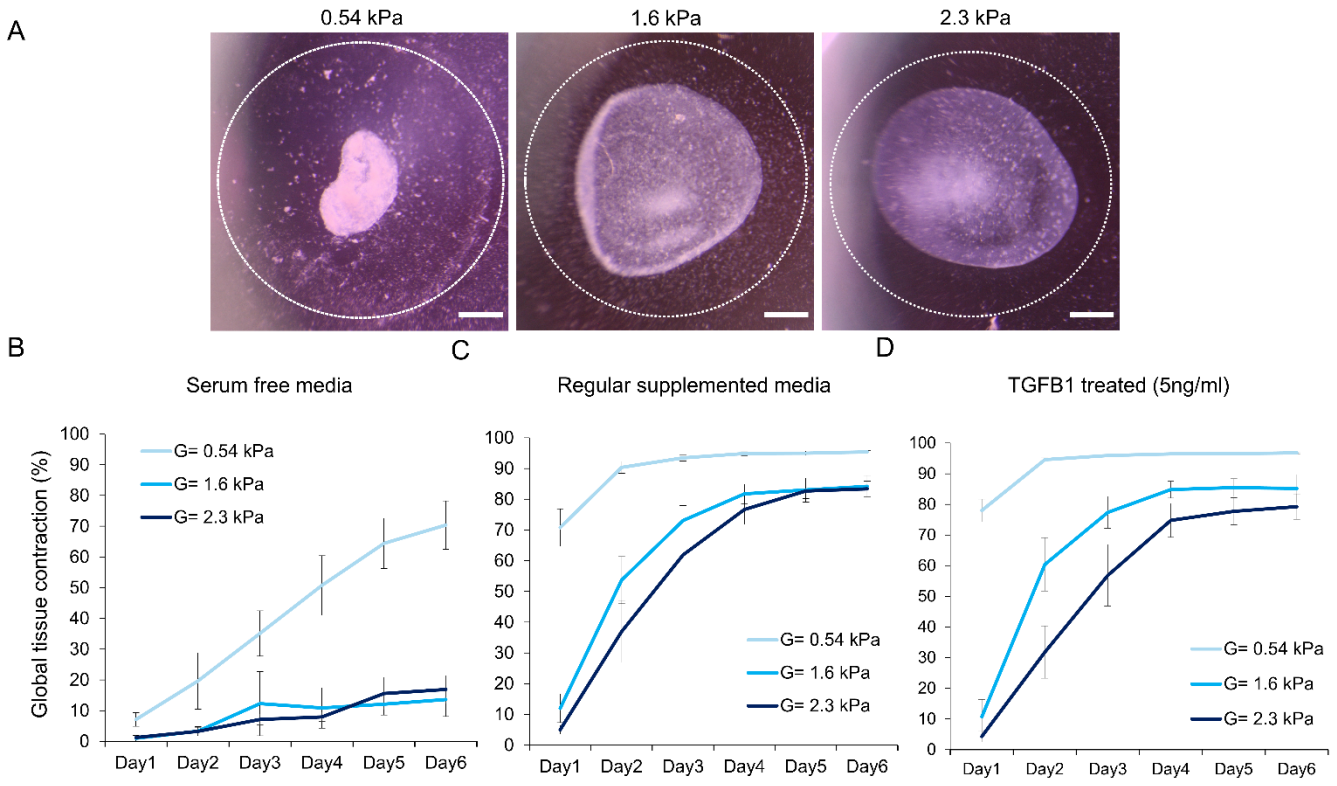

Figure 4. Microgel contraction as a function of time under various stiffnesses and soluble factors. (A) Representative contracted microgels at day 2 in regular supplemented media (white dashed line represents microgel at day 0; scale: 400 μm). Overall global microgel contraction time course over 6 days in (B) serum free conditions, (C) FBS supplemented media conditions, and (D) FBS supplemented media + 5ng/mL TGFβ-1 conditions (data presented as mean +/- standard deviation; n =6-12 microgels).

Microgel stiffness influences chemotherapy effectiveness

Given the responsiveness of this platform to soluble factors, we then sought to demonstrate the utility of stiffness-tunable microgels in a more conventional and industry-relevant assay. 3D culture has previously been demonstrated to have a strong protective effect against certain chemotherapeutics, compared to 2D cultures,[38] and 3D stiffness is known to have an effect on chemotherapeutic efficacy.[39] [40] Clinically, patients with low breast tissue stiffness also respond better to chemotherapy than those with high breast tissue stiffness,[41] suggesting that considering stiffness in early drug screening protocols would be an important factor in screening for the next generation of therapeutics. To determine whether stiffness may play a role in this process, and simultaneously demonstrate the utility of this platform for drug-screening, we designed a simple viability-based screen for MDA-MB-231 cells in stiffness-tunable gels against paclitaxel, a well-established chemotherapeutic agent. Breast tissue stiffness spans a shear modulus range from < 1 kPa in healthy tissue, to between 1 kPa and 3 kPa+ at the invasive front of disease.[42] The microgel formulations selected here may therefore model the stiffness evolution that occurs during breast cancer progression.

Breast cancer cells cultured in initially softer gels were more responsive to paclitaxel than cells in the initially stiffest gels, suggesting that increased stiffness has a small but statistically significant chemoprotective effect (Figure 5A) (Figure S8). Interestingly, this effect was not monotonic with stiffness.

The initially mid-range 1.6 kPa gels were more sensitive to all concentrations of paclitaxel than were each of the other gels, suggesting that an optimal stiffness exists at which certain drugs can be more effective. Stiffness did not influence viability due to the chemotherapeutic vehicle for delivery (Figure S9). As paclitaxel is selectively taken up by proliferating cells,[43] and stiffness is a known factor influencing proliferation,[8] we reasoned that stiffness-induced changes in proliferation may be responsible for this response. We therefore characterized the relative proliferation of cancer cells in this system, and found that increasing stiffness generally is associated with decreased proliferation, except in the 1.6 kPa gels which notably demonstrate the highest proliferative rates of all cultures tested (Figure 5B). Hence, differences in proliferation likely underlie the observed phenotypes.

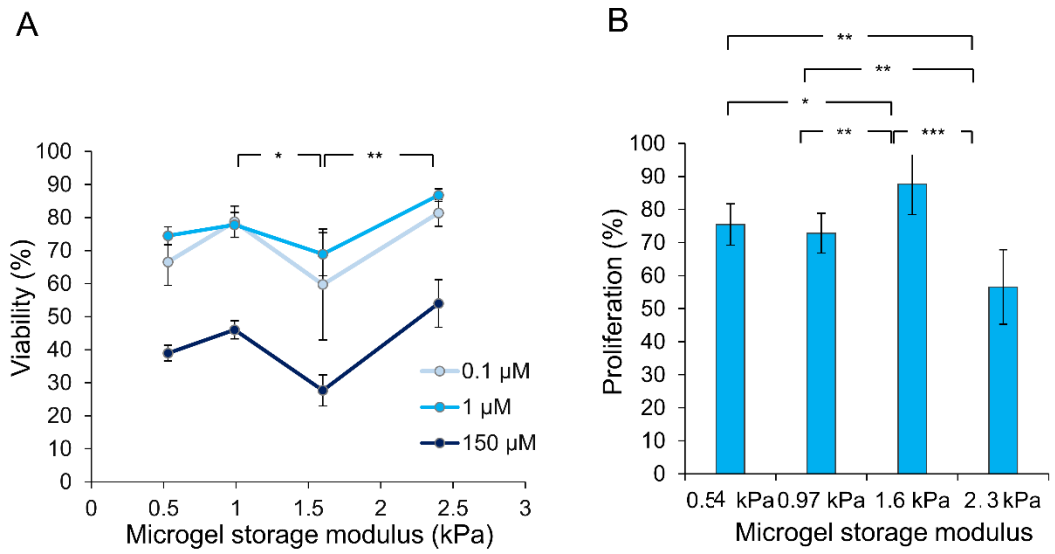

Figure 5. Breast cancer cell susceptibility to chemotherapy changes depends on microgel stiffness. (A) Live/dead analysis following 48 hours of exposure to Paclitaxel at a concentration of either 0.1 µM, 1 µM, or 150 µM. Presented significance reflects the lowest seen significance in 0.1 µM gels and all other concentrations display higher significance. For detailed significance, see Figure S8. (B) Ki67 staining illustrates the total percentage of cancer cells undergoing active proliferation within each microgel (data presented as mean +/- standard deviation; n =3-6 microgels; * $p < 0.05$; ** $p < 0.01$; *** p= 0.0001 by one-way ANOVA with Tukey post-hoc analysis).

Discussion

Blending collagen-alginate IPNs with the PEG and dextran polymers to induce phase separation was shown to support bioprinting microvolumes of stiffness-tunable biomaterials, and was demonstrated here as a robust, increased-throughput method for 3D cell culture capable of multiple biological assays. We specifically focused on morphological analysis of multiple cell types, implementation of a functional collagen contraction assay, and a demonstration of a scalable live/dead viability assay against a commonly used chemotherapeutic. In each of these assays, low biomaterial volumes allow for decreased costs in terms of materials, reduced cell number requirements, and as previously determined,[21] can support faster diffusion and equilibration of soluble factors than bulk gels, allowing dynamic or long-term cell culture studies. Furthermore, both automatable handling using a desktop liquid handling robot,

and compatibility with standard fluorescent and brightfield microscopy techniques indicate that these methods can be rapidly adopted by standard wet-labs with this basic infrastructure.

In addition to demonstrating the utility of this system, our experiments also present some interesting findings. As expected, increasing 3D biomaterial stiffness results in decreased cell spreading, but this relationship is not linear with stiffness. Interestingly, there is a small trend towards increased spread area at the mid-range of stiffness in alginate-doped gels (1.6 kPa), and although not statistically significant, this observation is consistent across multiple repeated experiments, and correlates with statistically significant increases in chemotherapeutic efficacy (Figure 5A) and proliferative percentage (Figure 5B). Given the well-known relationship between cell spread area and proliferation,[32 8] and the proliferation-based mechanism of action for paclitaxel,[43] these results are internally consistent and suggest that the increase in spread area at the mid-range of stiffness is a genuine effect. Our observations of increased formation of well-defined F-actin structures due to increased stiffness (Figure 3G) suggests that the increased matrix stiffness does allow enhanced tension generation at the binding site to increase spread area,[32] but a competing mechanism must be simultaneously restricting spread area, despite the formation of pro-spreading actin structures. This is likely due to recently developed descriptions of ECM fiber recruitment being required to increase local binding ligand density and therefore cell spreading.[44 26 4 23] Hence, our observations support the idea of increased fibrous matrix stiffness hindering the ability of a cell to deform and therefore recruit fibers, while simultaneously providing tension at the binding complex to prompt increases in spread area. Notably, pore size also decreases as stiffness increases and cell confinement also attenuates cell spread.[45] Our data therefore suggests a “sweet spot” of ideal stiffness for maximal cell spreading and proliferation.

Some limitations should also be considered in the use of this culture technology. Although the phase angle is conserved over the range of alginate concentrations tested here, the viscoelastic storage and loss moduli of these matrices cannot be independently controlled. Since viscoelastic characteristics impart important and biologically relevant cues in culture, future work should consider incorporating the tunable viscoelastic properties of alginate in modifying the collagen mechanical properties. Second, although our OMTC measurements do provide a measure of cellular-scale rigidity within the materials, we only perform these prior to cell seeding. As collagen gels are well established to stiffen during contraction,[37 46 47] these remodelled matrices likely effect cell functions differently. The effects of cell spreading and contraction on highly local mechanical properties within the matrix are unclear, and studying the effects of these dynamic properties, particularly using a variety of novel techniques to characterize stresses and mechanical properties within 3D matrices at this cellular length scale,[48 49 50] could provide valuable future insight into cell-environment interactions. Finally, while the ATPS technique is compatible with standard liquid handling tools, adoption into standard workflows will require careful characterization of the effects of PEG and dextran on the specific biological assay being developed.

Conclusions

The present platform provides the ability to tune 3D culture stiffness, while bioprinting directly into well-plates for high-throughput screening applications using readily-available liquid handling tools. Hence, this platform may easily be adopted for a variety of applications requiring high-throughput culture, and may be particularly beneficial for those involving limited or rare cell populations, multiple culture conditions, and testing of secreted or soluble factors; such as drug screening, personalized medicine, organoid formation, and stem cell differentiation, each of which have significant stiffness-related effects. Our findings highlight the importance of using stiffness-tunable 3D culture models in fundamental biological discovery, and simultaneously provide accessible strategies to achieve this.

Acknowledgements
This work was supported by the Canadian Cancer Society (Grants #704422, 706002) the Canadian Institutes of Health Research (Grant # 01871-000), the NSERC Discovery Grants program (RGPIN-2015-05512), and the Canada Research Chairs in Advanced Cellular Microenvironments to CM.

Competing Interests
The authors declare no competing interests.

Supporting Information
Complex moduli, loss moduli, and phase angle of the matrices as a function of alginate concentration, HS5 day 0 viability, cell aspect ratio of HS5 fibroblast cells within the microgels, fibroblast morphology cultured on top of the matrices in 2D, 2D versus 3D HS5 fibroblast morphology, diffuse versus defined F-actin expression, alternative graph displaying specific significances within chemotherapy screen, breast cancer cell viability on exposure to chemotherapy vehicle.

References
(1) Baker, B. M.; Chen, C. S. Deconstructing the Third Dimension – How 3D Culture Microenvironments Alter Cellular Cues. *J. Cell Sci.* **2012**, *125* (13), 3015. https://doi.org/10.1242/jcs.079509.
(2) Khavari, A.; Nydén, M.; Weitz, D. A.; Ehrlicher, A. J. Composite Alginate Gels for Tunable Cellular Microenvironment Mechanics. *Sci. Rep.* **2016**, *6* (1), 30854. https://doi.org/10.1038/srep30854.
(3) Berger, A. J.; Linsmeier, K. M.; Kreeger, P. K.; Masters, K. S. Decoupling the Effects of Stiffness and Fiber Density on Cellular Behaviors via an Interpenetrating Network of Gelatin-Methacrylate and Collagen. *Biomaterials* **2017**, *141*, 125–135. https://doi.org/10.1016/j.biomaterials.2017.06.039.
(4) Matera, D. L.; Wang, W. Y.; Smith, M. R.; Shikanov, A.; Baker, B. M. Fiber Density Modulates Cell Spreading in 3D Interstitial Matrix Mimetics. *ACS Biomater. Sci. Eng.* **2019**. https://doi.org/10.1021/acsbiomaterials.9b00141.
(5) Chaudhuri, O.; Koshy, S. T.; Branco da Cunha, C.; Shin, J.-W.; Verbeke, C. S.; Allison, K. H.; Mooney, D. J. Extracellular Matrix Stiffness and Composition Jointly Regulate the Induction of Malignant Phenotypes in Mammary Epithelium. *Nat Mater* **2014**, *13* (10), 970–978. http://dx.doi.org/10.1038/nmat4009
(6) Engler, A. J.; Sen, S.; Sweeney, H. L.; Discher, D. E. Matrix Elasticity Directs Stem Cell Lineage Specification. *Cell* **2006**, *126* (4), 677–689. https://doi.org/10.1016/j.cell.2006.06.044.
(7) Yeung, T.; Georges, P. C.; Flanagan, L. A.; Marg, B.; Ortiz, M.; Funaki, M.; Zahir, N.; Ming, W.; Weaver, V.; Janmey, P. A. Effects of Substrate Stiffness on Cell Morphology, Cytoskeletal Structure, and Adhesion. *Cell Motil.* **2005**, *60* (1), 24–34. https://doi.org/10.1002/cm.20041.
(8) Tilghman, R. W.; Cowan, C. R.; Mih, J. D.; Koryakina, Y.; Gioeli, D.; Slack-Davis, J. K.; Blackman, B. R.; Tschumperlin, D. J.; Parsons, J. T. Matrix Rigidity Regulates Cancer Cell Growth and Cellular Phenotype. *PLOS ONE* **2010**, *5* (9), e12905. https://doi.org/10.1371/journal.pone.0012905.
(9) Paszek, M. J.; Zahir, N.; Johnson, K. R.; Lakins, J. N.; Rozenberg, G. I.; Gefen, A.; Reinhart-King, C. A.; Margulies, S. S.; Dembo, M.; Boettiger, D.; Hammer, D. A.; Weaver, V. M. Tensional Homeostasis and the Malignant Phenotype. *Cancer Cell* **2005**, *8* (3), 241–254. https://doi.org/10.1016/j.ccr.2005.08.010.

(10) Ort, C.; Lee, W.; Kalashnikov, N.; Moraes, C. Disentangling the Fibrous Microenvironment: Designer Culture Models for Improved Drug Discovery. *Expert Opin. Drug Discov.* **2020**, 1–13. https://doi.org/10.1080/17460441.2020.1822815.

(11) Carvalho, M. R.; Lima, D.; Reis, R. L.; Oliveira, J. M.; Correlo, V. M. Anti-Cancer Drug Validation: The Contribution of Tissue Engineered Models. *Stem Cell Rev. Rep.* **2017**, 1–17. https://doi.org/10.1007/s12015-017-9720-x.

(12) Zustiak, S.; Nossal, R.; Sackett, D. L. Multiwell Stiffness Assay for the Study of Cell Responsiveness to Cytotoxic Drugs. *Biotechnol. Bioeng.* **2014**, *111* (2), 396–403. https://doi.org/10.1002/bit.25097.

(13) Cruz-Acuña, R.; Quirós, M.; Huang, S.; Siuda, D.; Spence, J. R.; Nusrat, A.; García, A. J. PEG-4MAL Hydrogels for Human Organoid Generation, Culture, and in Vivo Delivery. *Nat. Protoc.* **2018**, *13* (9), 2102–2119. https://doi.org/10.1038/s41596-018-0036-3.

(14) Gjorevski, N.; Sachs, N.; Manfrin, A.; Giger, S.; Bragina, M. E.; Ordóñez-Morán, P.; Clevers, H.; Lutolf, M. P. Designer Matrices for Intestinal Stem Cell and Organoid Culture. *Nature* **2016**, *539* (7630), 560–564. https://doi.org/10.1038/nature20168.

(15) Capeling, M. M.; Czerwinski, M.; Huang, S.; Tsai, Y.-H.; Wu, A.; Nagy, M. S.; Juliar, B.; Sundaram, N.; Song, Y.; Han, W. M.; Takayama, S.; Alsberg, E.; Garcia, A. J.; Helmrath, M.; Putnam, A. J.; Spence, J. R. Nonadhesive Alginate Hydrogels Support Growth of Pluripotent Stem Cell-Derived Intestinal Organoids. *Stem Cell Rep.* **2019**, *12* (2), 381–394. https://doi.org/10.1016/j.stemcr.2018.12.001.

(16) Ranga, A.; Girgin, M.; Meinhardt, A.; Eberle, D.; Caiazzo, M.; Tanaka, E. M.; Lutolf, M. P. Neural Tube Morphogenesis in Synthetic 3D Microenvironments. *Proc. Natl. Acad. Sci.* **2016**, *113* (44), E6831. https://doi.org/10.1073/pnas.1603529113.

(17) Ouyang, L.; Armstrong, J. P. K.; Lin, Y.; Wojciechowski, J. P.; Lee-Reeves, C.; Hachim, D.; Zhou, K.; Burdick, J. A.; Stevens, M. M. Expanding and Optimizing 3D Bioprinting Capabilities Using Complementary Network Bioinks. *Sci. Adv.* **2020**, *6* (38), eabc5529. https://doi.org/10.1126/sciadv.abc5529.

(18) Brassard, J. A.; Nikolaev, M.; Hübscher, T.; Hofer, M.; Lutolf, M. P. Recapitulating Macro-Scale Tissue Self-Organization through Organoid Bioprinting. *Nat. Mater.* **2020**. https://doi.org/10.1038/s41563-020-00803-5.

(19) Yang, X.; Lu, Z.; Wu, H.; Li, W.; Zheng, L.; Zhao, J. Collagen-Alginate as Bioink for Three-Dimensional (3D) Cell Printing Based Cartilage Tissue Engineering. *Mater. Sci. Eng. C* **2018**, *83*, 195–201. https://doi.org/10.1016/j.msec.2017.09.002.

(20) Datta, P.; Dey, M.; Ataie, Z.; Unutmaz, D.; Ozbolat, I. T. 3D Bioprinting for Reconstituting the Cancer Microenvironment. *Npj Precis. Oncol.* **2020**, *4* (1), 18. https://doi.org/10.1038/s41698-020-0121-2.

(21) Moraes, C.; Simon, A. B.; Putnam, A. J.; Takayama, S. Aqueous Two-Phase Printing of Cell-Containing Contractile Collagen Microgels. *Biomaterials* **2013**, *34* (37), 10.1016/j.biomaterials.2013.08.046. https://doi.org/10.1016/j.biomaterials.2013.08.046.

(22) Jiang, T.; Munguia-Lopez, J. G.; Gu, K.; Bavoux, M. M.; Flores-Torres, S.; Kort-Mascort, J.; Grant, J.; Vijayakumar, S.; De Leon-Rodriguez, A.; Ehrlicher, A. J.; Kinsella, J. M. Engineering Bioprintable Alginate/Gelatin Composite Hydrogels with Tunable Mechanical and Cell Adhesive Properties to Modulate Tumor Spheroid Growth Kinetics. *Biofabrication* **2019**, *12* (1), 015024. https://doi.org/10.1088/1758-5090/ab3a5c.

(23) Gillette, B. M.; Jensen, J. A.; Wang, M.; Tchao, J.; Sia, S. K. Dynamic Hydrogels: Switching of 3D Microenvironments Using Two-Component Naturally Derived Extracellular Matrices. *Adv. Mater.* **2010**, *22* (6), 686–691. https://doi.org/10.1002/adma.200902265.

(24) Cavo, M.; Caria, M.; Pulsoni, I.; Beltrame, F.; Fato, M.; Scaglione, S. A New Cell-Laden 3D Alginate-Matrigel Hydrogel Resembles Human Breast Cancer Cell Malignant Morphology, Spread and Invasion Capability Observed "in Vivo." *Sci. Rep.* **2018**, *8* (1), 5333. https://doi.org/10.1038/s41598-018-23250-4.

(25) Ledo, A. M.; Vining, K. H.; Alonso, M. J.; Garcia-Fuentes, M.; Mooney, D. J. Extracellular Matrix Mechanics Regulate Transfection and SOX9-Directed Differentiation of Mesenchymal Stem Cells. *Acta Biomater.* **2020**, *110*, 153–163. https://doi.org/10.1016/j.actbio.2020.04.027.

(26) Branco da Cunha, C.; Klumpers, D. D.; Li, W. A.; Koshy, S. T.; Weaver, J. C.; Chaudhuri, O.; Granja, P. L.; Mooney, D. J. Influence of the Stiffness of Three-Dimensional Alginate/Collagen-I Interpenetrating Networks on Fibroblast Biology. *Biomaterials* **2014**, *35* (32), 8927–8936. https://doi.org/10.1016/j.biomaterials.2014.06.047.

(27) Cao, H.; Lee, M. K. H.; Yang, H.; Sze, S. K.; Tan, N. S.; Tay, C. Y. Mechanoregulation of Cancer-Associated Fibroblast Phenotype in Three-Dimensional Interpenetrating Hydrogel Networks. *Langmuir* **2018**. https://doi.org/10.1021/acs.langmuir.8b02649.

(28) Lee, K. Y.; Mooney, D. J. Alginate: Properties and Biomedical Applications. *Prog. Polym. Sci.* **2012**, *37* (1), 106–126. https://doi.org/10.1016/j.progpolymsci.2011.06.003.

(29) Beachley, V. Z.; Wolf, M. T.; Sadtler, K.; Manda, S. S.; Jacobs, H.; Blatchley, M. R.; Bader, J. S.; Pandey, A.; Pardoll, D.; Elisseeff, J. H. Tissue Matrix Arrays for High-Throughput Screening and Systems Analysis of Cell Function. *Nat. Methods* **2015**, *12* (12), 1197–1204. https://doi.org/10.1038/nmeth.3619.

(30) Giancotti, F. G.; Ruoslahti, E. Integrin Signaling. *Science* **1999**, *285* (5430), 1028. https://doi.org/10.1126/science.285.5430.1028.

(31) Puig-De-Morales, M.; Grabulosa, M.; Alcaraz, J.; Mullol, J.; Maksym, G. N.; Fredberg, J. J.; Navajas, D. Measurement of Cell Microrheology by Magnetic Twisting Cytometry with Frequency Domain Demodulation. *J. Appl. Physiol.* **2001**, *91* (3), 1152–1159. https://doi.org/10.1152/jappl.2001.91.3.1152.

(32) Engler, A.; Bacakova, L.; Newman, C.; Hategan, A.; Griffin, M.; Discher, D. Substrate Compliance versus Ligand Density in Cell on Gel Responses. *Biophys. J.* **2004**, *86* (1), 617–628. https://doi.org/10.1016/S0006-3495(04)74140-5.

(33) Clapham, D. E. Calcium Signaling. *Cell* **2007**, *131* (6), 1047–1058. https://doi.org/10.1016/j.cell.2007.11.028.

(34) Vining, K. H.; Stafford, A.; Mooney, D. J. Sequential Modes of Crosslinking Tune Viscoelasticity of Cell-Instructive Hydrogels. *Biomaterials* **2019**, *188*, 187–197. https://doi.org/10.1016/j.biomaterials.2018.10.013.

(35) Balestrini, J. L.; Chaudhry, S.; Sarrazy, V.; Koehler, A.; Hinz, B. The Mechanical Memory of Lung Myofibroblasts. *Integr. Biol.* **2012**, *4* (4), 410–421. https://doi.org/10.1039/c2ib00149g.

(36) Grinnell, F.; Petroll, W. M. Cell Motility and Mechanics in Three-Dimensional Collagen Matrices. *Annu. Rev. Cell Dev. Biol.* **2010**, *26* (1), 335–361. https://doi.org/10.1146/annurev.cellbio.042308.113318.

(37) Han, Y. L.; Ronceray, P.; Xu, G.; Malandrino, A.; Kamm, R. D.; Lenz, M.; Broedersz, C. P.; Guo, M. Cell Contraction Induces Long-Ranged Stress Stiffening in the Extracellular Matrix. *Proc. Natl. Acad. Sci. U. S. A.* **2018**, *115* (16), 4075–4080. https://doi.org/10.1073/pnas.1722619115.

(38) Lovitt, C. J.; Shelper, T. B.; Avery, V. M. Evaluation of Chemotherapeutics in a Three-Dimensional Breast Cancer Model. *J. Cancer Res. Clin. Oncol.* **2015**, *141* (5), 951–959. https://doi.org/10.1007/s00432-015-1950-1.

(39) Joyce, M. H.; Lu, C.; James, E. R.; Hegab, R.; Allen, S. C.; Suggs, L. J.; Brock, A. Phenotypic Basis for Matrix Stiffness-Dependent Chemoresistance of Breast Cancer Cells to Doxorubicin. *Front. Oncol.* **2018**, *8*, 337–337. https://doi.org/10.3389/fonc.2018.00337.

(40) Shin, J.-W.; Mooney, D. J. Extracellular Matrix Stiffness Causes Systematic Variations in Proliferation and Chemosensitivity in Myeloid Leukemias. *Proc. Natl. Acad. Sci. U. S. A.* **2016**, *113* (43), 12126–12131. https://doi.org/10.1073/pnas.1611338113.

(41) Jing, H.; Cheng, W.; Li, Z.-Y.; Ying, L.; Wang, Q.-C.; Wu, T.; Tian, J.-W. Early Evaluation of Relative Changes in Tumor Stiffness by Shear Wave Elastography Predicts the Response to Neoadjuvant Chemotherapy in Patients With Breast Cancer. *J. Ultrasound Med.* **2016**, *35* (8), 1619–1627. https://doi.org/10.7863/ultra.15.08052.

(42) Acerbi, I.; Cassereau, L.; Dean, I.; Shi, Q.; Au, A.; Park, C.; Chen, Y.; Liphardt, J.; Hwang, E.; Weaver, V. Human Breast Cancer Invasion and Aggression Correlates with ECM Stiffening and Immune Cell Infiltration. *Integr. Biol. Quant. Biosci. Nano Macro* **2015**, *7* (10), 1120–1134. https://doi.org/10.1039/c5ib00040h.

(43) Weaver, B. A. How Taxol/Paclitaxel Kills Cancer Cells. *Mol. Biol. Cell* **2014**, *25* (18), 2677–2681. https://doi.org/10.1091/mbc.E14-04-0916.

(44) Baker, B. M.; Trappmann, B.; Wang, W. Y.; Sakar, M. S.; Kim, I. L.; Shenoy, V. B.; Burdick, J. A.; Chen, C. S. Cell-Mediated Fibre Recruitment Drives Extracellular Matrix Mechanosensing in Engineered Fibrillar Microenvironments. *Nat. Mater.* **2015**, *14* (12), 1262–1268. https://doi.org/10.1038/nmat4444.

(45) Ranamukhaarachchi, S. K.; Modi, R. N.; Han, A.; Velez, D. O.; Kumar, A.; Engler, A. J.; Fraley, S. I. Macromolecular Crowding Tunes 3D Collagen Architecture and Cell Morphogenesis. *Biomater. Sci.* **2019**, *7* (2), 618–633. https://doi.org/10.1039/C8BM01188E.

(46) Asmani, M.; Velumani, S.; Li, Y.; Wawrzyniak, N.; Hsia, I.; Chen, Z.; Hinz, B.; Zhao, R. Fibrotic Microtissue Array to Predict Anti-Fibrosis Drug Efficacy. *Nat. Commun.* **2018**, *9* (1), 2066. https://doi.org/10.1038/s41467-018-04336-z.

(47) Calvo, F.; Ege, N.; Grande-Garcia, A.; Hooper, S.; Jenkins, R. P.; Chaudhry, S. I.; Harrington, K.; Williamson, P.; Moeendarbary, E.; Charras, G.; Sahai, E. Mechanotransduction and YAP-Dependent Matrix Remodelling Is Required for the Generation and Maintenance of Cancer-Associated Fibroblasts. *Nat. Cell Biol.* **2013**, *15* (6), 637–646. https://doi.org/10.1038/ncb2756.

(48) Lee, W.; Kalashnikov, N.; Mok, S.; Halaoui, R.; Kuzmin, E.; Putnam, A. J.; Takayama, S.; Park, M.; McCaffrey, L.; Zhao, R.; Leask, R. L.; Moraes, C. Dispersible Hydrogel Force Sensors Reveal Patterns of Solid Mechanical Stress in Multicellular Spheroid Cultures. *Nat. Commun.* **2019**, *10* (1), 144. https://doi.org/10.1038/s41467-018-07967-4.

(49) Mok, S.; Al Habyan, S.; Ledoux, C.; Lee, W.; MacDonald, K. N.; McCaffrey, L.; Moraes, C. Mapping Cellular-Scale Internal Mechanics in 3D Tissues with Thermally Responsive Hydrogel Probes. *Nat. Commun.* **2020**, *11* (1), 4757. https://doi.org/10.1038/s41467-020-18469-7.

(50) Khavari, A.; Ehrlicher, A. J. Nuclei Deformation Reveals Pressure Distributions in 3D Cell Clusters. *PLOS ONE* **2019**, *14* (9), e0221753. https://doi.org/10.1371/journal.pone.0221753.

For Table of Contents Use Only

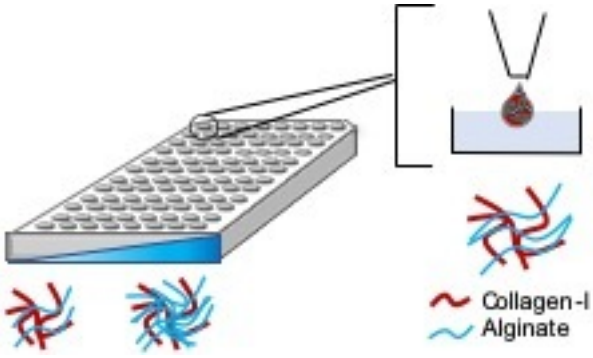

Bioprintable, stiffness-tunable collagen-alginate microgels for increased throughput 3D cell culture studies.

Carley Ort, Yimai Chen, Ajinkya Ghagre, Allen Ehrlicher and Christopher Moraes